





Article

Optical and Photodetection Properties of ZnO Nanoparticles Recovered from Zn Dross

Lina Jaya Diguna ^{1,*}, Aprilia Dyah Fitriani ², Beta Riana Liasari ³, Gerald Ensang Timuda ³, Wahyu Bambang Widayatno ³, Agus Sukarto Wismogroho ³, Shuwen Zeng ^{4,*}, Muhammad Danang Birowosuto ^{1,5} and Muhamad Ikhlasul Amal ^{6,*}

- ¹ Department of Renewable Energy Engineering, Universitas Prasetiya Mulya, Kavling Edutown I.1, Jl. BSD Raya Utama, BSD City, Tangerang 15339, Indonesia; mbirowosuto@ntu.edu.sg
 - ² Collaborative STEM Laboratories, Universitas Prasetiya Mulya, Kavling Edutown I.1, Jl. BSD Raya Utama, BSD City, Tangerang 15339, Indonesia; apriladyahfitriani@gmail.com
 - ³ Research Center for Physics, Indonesian Institute of Sciences, Bld. 440/442, PUSPIPTEK Serpong, Tangerang Selatan 15314, Indonesia; betariana7@gmail.com (B.R.L.); gera001@lipi.go.id (G.E.T.); wahy012@lipi.go.id (W.B.W.); agus046@lipi.go.id (A.S.W.)
 - ⁴ XLIM Research Institute, UMR 7252 CNRS/University of Limoges, 123, Avenue Albert Thomas, 87060 Limoges CEDEX, France
 - ⁵ CINTRA UMI CNRS/NTU/THALES 3288, Research Techno Plaza, 50 Nanyang Drive, Border X Block, Level Singapore 637553, Singapore
 - ⁶ Research Center for Metallurgy and Materials, Indonesian Institute of Sciences, PUSPIPTEK Tangerang Selatan, Banten 15314, Indonesia
- * Correspondence: lina.diguna@prasetiyamulya.ac.id (L.J.D.); zeng@xlim.fr (S.Z.); muha137@lipi.go.id (M.I.A.)

Abstract: In this study, we report the synthesis of ZnO nanoparticles from Zn dross via hydrometallurgical method by using acetic acid as a leaching agent. D205 dye molecules were then adsorbed onto Zn dross originated ZnO nanoparticle film. The optical absorption confirms the photosensitization of the synthesized ZnO nanoparticles with dye. The photoluminescence spectra reveal the excitonic- and defect-related emission of ZnO nanoparticles. Compared to ZnO nanoparticles only, the longer emission lifetime of ZnO nanoparticles with adsorbed dye indicates the transfer of photoexcited electrons from dye to the ZnO nanoparticles. Furthermore, photodetection characterization of ZnO film show the enhanced current density with the presence of dye under simulated solar illumination, while that measured at dark is similar in both films with and without dye. This result confirms the potentiality of Zn dross to be recycled into valuable ZnO nanoparticles particularly for the applications in the visible light region, especially for sensing.

Keywords: zinc oxide; zinc dross; optical properties; photodetection properties



Citation: Diguna, L.J.; Fitriani, A.D.; Liasari, B.R.; Timuda, G.E.; Widayatno, W.B.; Wismogroho, A.S.; Zeng, S.; Birowosuto, M.D.; Amal, M.I. Optical and Photodetection Properties of ZnO Nanoparticles Recovered from Zn Dross. *Crystals* **2021**, *11*, 6. <https://dx.doi.org/10.3390/cryst11010006>

Received: 23 November 2020

Accepted: 21 December 2020

Published: 23 December 2020

Publisher's Note: MDPI stays neutral with regard to jurisdictional claims in published maps and institutional affiliations.



Copyright: © 2020 by the authors. Licensee MDPI, Basel, Switzerland. This article is an open access article distributed under the terms and conditions of the Creative Commons Attribution (CC BY) license (<https://creativecommons.org/licenses/by/4.0/>).

1. Introduction

Wide band gap semiconductors have been considered as active materials in many applications such as light-emitting devices [1–3], solar cells [4–6], and photocatalysis [7–9]. One of the wide band gap semiconductors is ZnO with the band gap of 3.1–3.3 eV, and thus absorbing light only in the UV region [10]. Many studies have been conducted to synthesize ZnO nanostructures with different morphologies such as nanoparticles [11], nanorods [12], nanotubes [13], and nanowires [14]. Tuning the properties of ZnO materials has also been pursued by doping with other elements [15,16]. These approaches were carried out intentionally by using specific chemical precursors to allow preferentially the formation of high quality of ZnO nanomaterials.

On the other hand, the wide exploitation of Zn in industries has produces waste, i.e., Zn dross. As a byproduct of the galvanization process, zinc dross can contain more than 80% metallic zinc [17]. This valuable high content of zinc in the dross has motivated to recover it and even to use for advanced materials. We have previously conducted leaching

process of zinc dust using oxalic acid by hydrometallurgical method [18]. Based on our previous study, zinc element in the dross presents in the form of its oxide with some metal impurities, in which the metal composition mainly consisted of 96.3 wt% Zn and 3.6 wt% Fe. To scale-up the process for commercial applications, consideration should be taken in making this synthesis more viable in terms of cost incurred. Therefore, this study aims to utilize zinc dross from industrial byproducts to synthesize ZnO nanoparticles by using the economically viable acetic acid as a leaching agent in sensing. To investigate the possible application in visible region, dye is adsorbed on the surface of ZnO nanoparticle film followed the characterization of its absorption and photoluminescence (PL) properties. Time-resolved PL is also used to examine the charge carrier dynamics on this dye-adsorbed ZnO nanoparticles. The photodetection properties of both films with and without dye are also characterized by measuring current density-voltage curves at the dark and under simulated solar illumination.

2. Materials and Methods

2.1. Sample Preparation

ZnO nanoparticles were synthesized by using Zn dross as the raw material, in which the recovery of zinc element contained in the dross was conducted via the hydrometallurgical method [18]. The synthesis process of ZnO nanoparticles from Zn dross is illustrated in Figure S1 (see supplementary materials). Initially, 50 g of zinc dross was added to 500 mL of 4 M acetic acid solution and the mixture was stirred at 60 °C for 2 h. During the leaching process, the metal elements are extracted through dissolution in acid solution, producing the solution containing zinc ion and some unwanted metal ions, which are also dissolved. The solution with dissolved metal elements was separated from the residues by filtration. 100 mL of 25% ammonia solution was then added drop by drop to the filtrate in order to precipitate the metal impurities such as Fe. The formed precipitate was filtrated to separate it from the zinc acetate solution. Furthermore, 25 mL of zinc acetate filtrate was added with 10 mL distilled water, and 25 mL of 4 M sodium hydroxide (NaOH) solution was then added drop by drop to the zinc acetate solution under stirring at 60 °C until a white precipitate of ZnO was formed. After drying the white precipitate in the oven for 60 min at 185 °C, the sample was ground, resulting ZnO powder.

The thin film of synthesized ZnO was fabricated by the method previously reported [19,20], where 50 mg of synthesized ZnO powder was mixed with 20 mg of polyethylene glycol (PEG) having molecular weight of 3400 and 1.5 mL acetylacetone. The resulted paste was applied onto fluorine-doped tin oxide (FTO) coated glass using Scotch tape as a frame and spacer. Excess solution was raked off with a glass rod. The resulting film was then dried in air at room temperature and subsequently heated at 400 °C for 1 h. Dye adsorption on ZnO film was conducted by immersing the film in 0.5 mM D205 dye solution in tert-butanol:acetonitrile 1:1 mixture for 1 h. Gold (Au) coating was then performed on the films with and without dye adsorption as an electrical contact.

2.2. Measurements

ZnO powder was characterized by using X-ray diffractometer (Rigaku Smartlab, Rigaku Corporation, Tokyo, Japan, anode material is Cu with $K\alpha$ 1.5406 Å) to determine its composition, size, and formed structure. Microstructure observation was done by using scanning electron microscope (LEO 1550 Gemini, Carl Zeiss AG, Oberkochen, Germany). Absorption spectra were taken using ultraviolet–visible light (UV-vis) spectrometer (UV-2450, Shimadzu Corporation, Kyoto, Japan). In PL measurement, a 266 nm pulse laser (VisUV, PicoQuant GmbH, Berlin, Germany) with a line width of 15 ps and a repetition rate of 10 MHz was focused on samples with a microscope objective (Olympus PLN 40X (NA = 0.65), Olympus Corporation, Tokyo, Japan). The focused laser beam has a diameter of ≈ 1 μm . The PL signal was recorded by spectrometer (AvaSpec-HSC1024x58TEC-EVO, Avantes BV Apeldoorn, The Netherlands). Time-resolved PL measurement was carried out using single-photon avalanche photodiode (MPD, Picoquant GmbH, Berlin,

Germany) connected to a time-correlated single-photon counting acquisition module (TCC900, Edinburgh Instruments Ltd., Livingston, United Kingdom). Current density-voltage (J-V) characteristics were measured in the dark and under a solar simulator with AM1.5G filter by using a source measurement unit (Keithley 2400, Tektronix Inc., OR, USA). All samples were tested in ambient conditions and a simulated light intensity with the spot size diameter of 3 mm was adjusted to 100 mW/cm^2 calibrated with an optical power meter (PM100D, Thorlabs Inc., Newton, NJ, USA). In order to allow the measurement in parallel metal-semiconductor-metal configuration, each sample surface was divided into two regions by scratching.

3. Results and Discussion

Typical X-ray diffraction (XRD) pattern of the obtained particles is shown in Figure 1a, indicating the formation of hexagonal ZnO particles with space group of P63mc. The peaks in XRD pattern are in conformance with the database values for ZnO (JCPDS -361451). During the leaching process of zinc dross, zinc and other metal impurities are dissolved in acetic acid solution. The selective separation of Zn with other metals occurs with the precipitation of metal impurities by the addition of ammonium hydroxide. By adding the NaOH to the Zn acetate precursor, ZnO particles are formed. The data taken in XRD also shows ZnO nanoparticles with the crystallite size ranging from 30 nm to 70 nm. SEM images of ZnO film are shown in Figure 1b and Figure S2, in which the corresponding grain size distribution histogram in Figure S3 shows the average grain of about 180 nm in both horizontal and vertical diameters. This confirms that one grain or secondary particle in SEM contains several crystallites.

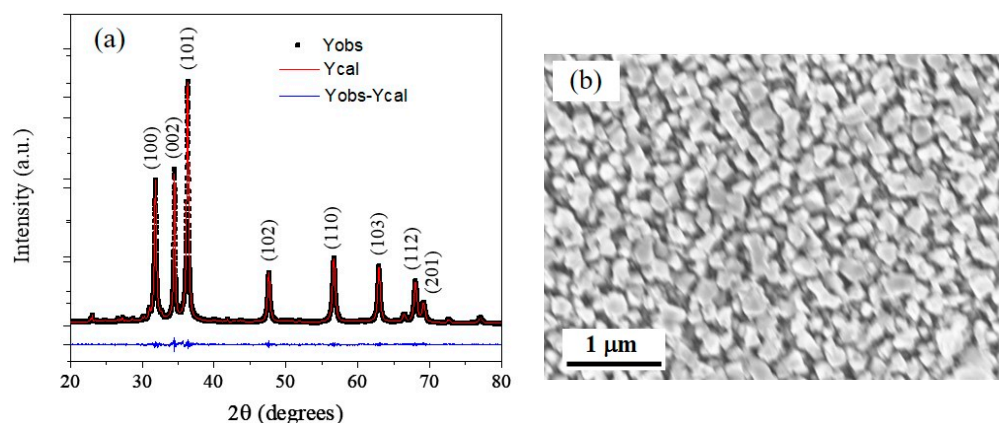


Figure 1. (a) X-ray diffraction pattern and (b) scanning electron microscope image of zinc dross originated ZnO nanoparticle film.

The absorption spectra of ZnO nanoparticle films with and without dye adsorption are shown in Figure 2a, in which the spectra are normalized at 300 nm. For the ZnO nanoparticle film, the absorption spectrum reveals the shoulder at about 360 nm, which corresponds to the absorption band of ZnO nanoparticles [21]. As shown from the Tauc plot in Figure S4, the band gap of synthesized ZnO is determined to be 3 eV (413 nm), which is higher compared to that reported band gap value of 2.88 eV for ZnO thin film [22]. With the dye adsorption on ZnO nanoparticles, this shoulder disappears and on the other hand the absorption in the visible region is appeared with the peak of 520 nm. This peak corresponds to the dye optical absorption since no absorption peak in the visible region is observed for ZnO only. The disappearance of shoulder might be caused by the absorption overlapping between D205 and ZnO considering the D205 absorption peak at 387 nm which is attributed to a mixture of the intermolecular charge transfer (ICT) and the π - π^* excitation from HOMO to LUMO +1. On the other hand, the absorption peak in the visible region, has a good agreement with the reported peak absorption at around 516 nm for D205-anchored ZnO nanoparticles, which is blue shifted from the absorption peak of D205 solution at

530 nm, ascribed the ICT transition from HOMO to LUMO, due to the moderate interaction between dye molecule and ZnO surface [23]. The appearance of visible absorption indicates the photosensitization of ZnO nanoparticles with adsorbed D205 dye molecules. Upon light absorption, the charge carriers are excited to the higher energy levels and later lose their energy through the relaxation process and finally fall back down to the ground state. PL spectroscopy can be used to study the radiative relaxation. Figure 2b shows the PL spectra of ZnO nanoparticle film with dye adsorption (red-colored) and without dye adsorption (black-colored) by using the excitation of 266 nm pulse laser with the pulse width of 15 ps. Both samples with and without dye adsorption have emission peak at 387 nm relatively with the same intensity, indicating the radiative recombination which belongs to excitonic emission of ZnO and not D205. This strongly correlates that D205 dye has no luminescence peak at wavelength less than 550 nm [24]. For ZnO nanoparticle sample, we also observed another emission peak at longer wavelength, i.e., 610 nm. This emission peak in the visible region may be related to the luminescent point defects, i.e., either a surface oxygen vacancy center or zinc vacancy center [25]. Furthermore, this emission peak is red-shifted to 625 nm with the higher intensity (around three times) with the dye adsorption on ZnO surface. It is possibly due to the strong bonding at the interface between ZnO and dye molecules which shifts the defect levels energetically and reorganize the interfacial charge [26]. Furthermore, the higher emission intensity with the dye adsorption indicates the effective electron transfer from dye molecules to ZnO thus contributing to the higher intensity. The emission peak in the visible region was also reported for D205-anchored ZnO particles, which were synthesized from high purity chemical precursors [24].

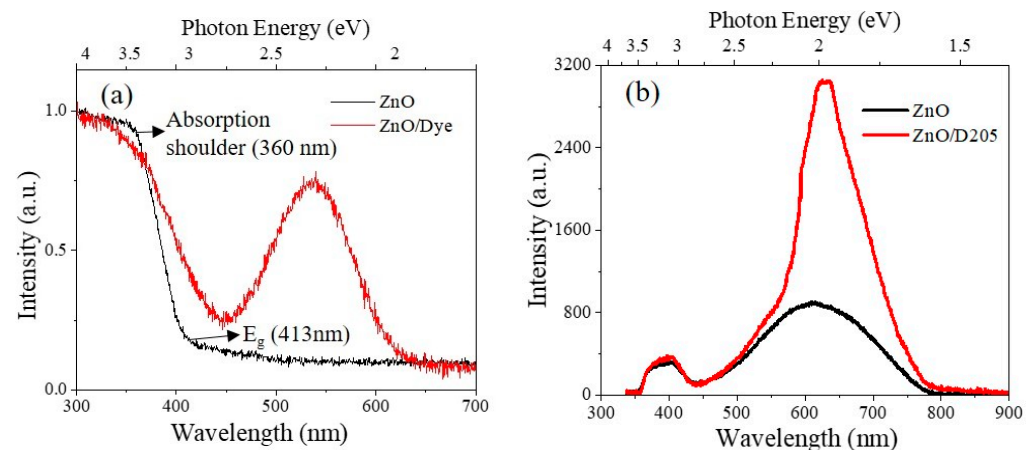


Figure 2. (a) Absorption and (b) photoluminescence (PL) spectra of the zinc dross originated ZnO nanoparticle films with (red-colored) and without (black-colored) dye adsorption.

To investigate the interfacial electron transfer between D205 dye and ZnO nanoparticles originated from Zn dross, the time-resolved PL decay measurements were taken at 400 nm and 600 nm. Figure 3 shows time-resolved PL decay curves at 400 nm and 600 nm emission wavelength recorded for ZnO nanoparticles with and without dye adsorption. The decays were then fitted with exponential decay in order to determine the emission lifetimes. The fitting results are shown in Table 1, with all cases the lifetime can be characterized as being in the nanoseconds range. For the emission at 400 nm, the decays of both ZnO nanoparticles with and without dye adsorption could be satisfactorily fit by bi-exponential function. The decay of ZnO nanoparticles only has decay constants of 0.45 ns and 3.00 ns with relative amplitudes of 46% and 54%; while the decay of ZnO nanoparticles with dye has decay constant of 0.56 ns and 3.79 ns with relative amplitudes of 57% and 43%, respectively. The average emission lifetime at 400 nm becomes slower from 1.82 to 1.95 ns as adsorption of dye on ZnO nanoparticles. Upon photoexcitation, the electrons are excited from HOMO to LUMO of the dye. These photoexcited electrons are then transferred to the conduction band of ZnO nanoparticles. These additional photoexcited electrons in ZnO

causes the longer lifetime of photoexcited electrons in ZnO. At emission at lower energy of 600 nm, the decay of ZnO nanoparticles could be well described by a tri-exponential function with decay constants of 0.24 ns, 1.34 ns, and 9.00 ns with relative amplitudes of 22%, 50%, and 28%, respectively. From emission at higher energy of 400 nm to lower energy of 600 nm, the averaged time decay constant for ZnO nanoparticles has been found to increase from 1.82 ns to 3.38 ns. This indicates that the defect-related emission lifetime of ZnO nanoparticles is almost double that those of excitonic-related emission. With the dye adsorption, the emissions at 600 nm could be satisfactorily fit by bi-exponential function, like the emission at 400 nm for both ZnO nanoparticles with and without dye. The decay constants of sample with dye adsorption were found to be 0.91 ns and 8.34 ns with relative amplitudes of 57% and 43%, respectively. At emission of 600 nm, longer lifetime was also found from 3.38 ns to 4.09 ns as dye molecules adsorbed on nanoparticle surface, due to the transferred of photoexcited electrons from the LUMO of dye to the conduction band of ZnO nanoparticles. From emission at higher energy of 400 nm to lower energy of 600 nm, the averaged time decay constant for ZnO nanoparticles with dye has also been found to be almost double from 1.95 ns to 4.09 ns, like those of ZnO nanoparticles only. From 400 to 600 nm, the comparable degree of emission lifetime shortening for both ZnO nanoparticles with and without dye adsorption clearly shows that the observed lifetimes belong to the excitonic- and defect-related emission of ZnO nanoparticles, or in other word there is electron transfer from dye to ZnO nanoparticles synthesized from Zn cross.

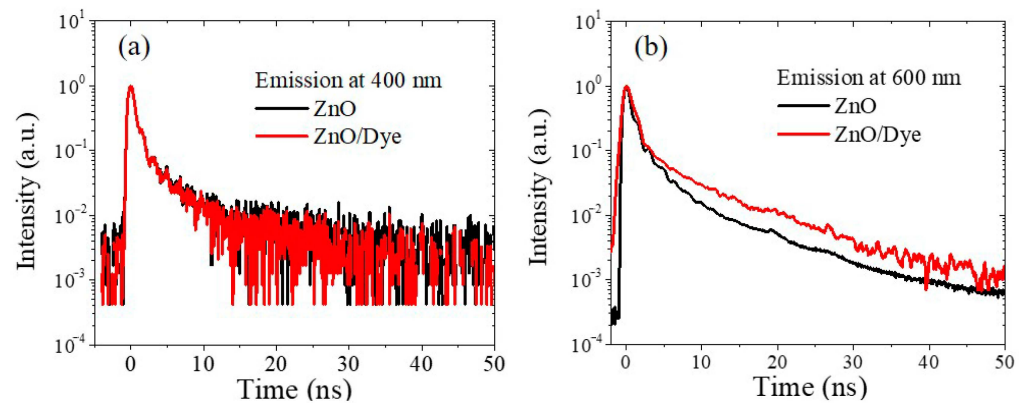


Figure 3. Normalized time-resolved PL spectra at emission peak of (a) 400 nm and (b) 600 nm of the zinc cross-originated ZnO nanoparticle films with (red-colored) and without (black-colored) dye adsorption.

Table 1. Kinetic parameters of emission decay analysis.

Thin Film	Emission Peak	τ_1 (ns)	a_1	τ_2 (ns)	a_2	τ_3 (ns)	a_3	τ_{ave} (ns)
ZnO	400 nm	0.45	46%	3.00	54%			1.82
ZnO/dye	400 nm	0.56	57%	3.79	43%			1.95
ZnO	600 nm	0.24	22%	1.34	50%	9.00	28%	3.38
ZnO/dye	600 nm	0.91	57%	8.34	43%			4.09

The photodetection properties of both ZnO nanoparticle films with and without dye were characterized by applying a voltage between the gold contact on these two regions and measuring the current flowing through parallel metal–semiconductor–metal configuration as shown in the inset of Figure 4a. Here, the current measured is converted into current density by dividing it by area of illuminating light spot in order to know the effect of illumination. The current density–voltage (J - V) curves of both films without and with dye are shown in Figure 4a,b, respectively. Measurements were conducted in forward bias and then back to zero intersection. All the curves showed Schottky barrier formation between metal–semiconductor interface. Schottky barrier heights of Au/ZnO

interface could range from 0 to 1.2 eV, depending on the crystal, the surface preparation, and the conditions under which the contact is formed [27]. At the dark, similar J-V curves could be clearly seen for those with and without dye, indicating no significant effects on the corresponding dark current with the presence of dye. Under illumination, the higher current was measured relative to the dark for both films due to the additional carriers generated under illumination. The observed trend at the dark and under illumination like to those reported for the ZnO film deposited using DC-unbalanced magnetron sputtering (DC-UBMS) with silver as the metal contact measured under UV light irradiation [28]. Furthermore, the enhancement of the photocurrent with the presence of dye is higher than that without dye because dye absorbs visible light while ZnO only absorbs only UV light under irradiance of solar simulator, so the visible light-excited carriers in dye are then transferred to the conduction band of ZnO. The addition of visible light-excited carriers in dye to the UV light-excited carriers in the conduction band of ZnO makes the larger photo-generated carriers and subsequently the more sensitive photodetection with the dye.

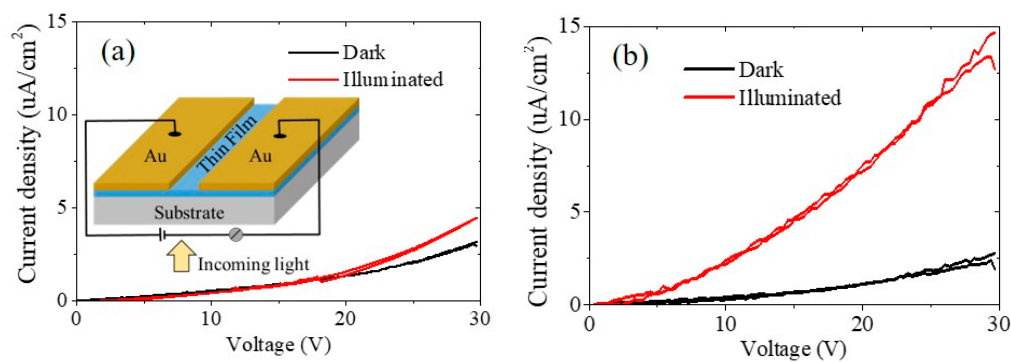


Figure 4. Current density–voltage (J-V) curves in the dark (black-colored) and under simulated solar illumination (red-colored) of zinc dross-originated ZnO nanoparticle film (a) without and (b) with dye adsorption. The inset in (a) is the schematic illustration of parallel metal-semiconductor-metal configuration.

The observed visible light absorption and transfer of photoexcited electrons from dye molecules to ZnO nanoparticles reveals the dye sensitization and the potential application of Zn dross originated ZnO nanoparticles in visible light region. In current synthesis process, optimization of the resulted ZnO nanoparticles from Zn dross should be carried out in terms of acid solution concentration, temperature, and duration. After the synthesis process, certain treatment such as meshing might also be taken in order to selectively obtain the certain size of the ZnO particles.

4. Conclusions

ZnO nanoparticles have been successfully synthesized from ZnO dross via hydrometallurgical method. During the leaching process, acetic acid could recover zinc in the form of zinc acetate which is then used to synthesize ZnO nanoparticles. XRD and SEM investigations confirm the synthesized ZnO particles in the size of nm order and the agglomeration of ZnO nanoparticles forming secondary particles with larger size, respectively. The optical absorption has revealed the photosensitization of the synthesized ZnO nanoparticles with D205 dye adsorption. The PL spectra has two emission peaks corresponding to the reveal the excitonic- and defect-related recombination in ZnO nanoparticles. With the dye adsorption, ZnO nanoparticles has showed the longer emission lifetime relative to those without dye, confirming the transfer of photoexcited electrons from dye to the ZnO nanoparticles. Moreover, photodetection characterization of ZnO film has showed the enhanced photocurrent with the presence of dye under simulated solar illumination, while at the dark both ZnO films with and without dye revealed similar characteristics. The results obtained in this study shows the potentiality of Zn dross to be recycled into more valued materials,

i.e., ZnO nanoparticles, with the properties comparable with those purposely synthesized from high purity raw chemicals. Further investigation should be considered in order to utilize in various real applications such as photocatalysis, emitting devices or solar cells, detectors, and even for sensing devices.

Supplementary Materials: The following are available online at <https://www.mdpi.com/2073-4352/11/1/6/s1>, Figure S1: Schematic illustration of synthesis process of ZnO nanoparticles from Zn dross. Figure S2. SEM images of ZnO nanoparticle film. Figure S3. (a) Illustration of grain size with vertical and horizontal measurements. Zn dross-originated ZnO grain size distribution histograms of (b) horizontal and (c) vertical diameters determined from the SEM image. Figure S4. Tauc plot for Zn dross-originated ZnO nanoparticles as a function of photon energy, revealing the band gap energy of 3 eV (413 nm).

Author Contributions: Conceptualization, L.J.D. and M.I.A.; methodology, L.J.D. and M.I.A.; investigation, A.D.F., W.B.W., A.S.W., S.Z., and M.D.B.; resources, A.D.F., B.R.L., and G.E.T.; formal analysis, L.J.D., M.D.B., and M.I.A.; writing—original draft preparation, L.J.D. and M.D.B.; writing—review and editing, L.J.D., S.Z., and M.I.A.; supervision, L.J.D. and M.I.A. All authors have read and agreed to the published version of the manuscript.

Funding: This work was supported by Universitas Prasetya Mulya and the Indonesian Ministry for Research, Technology and Higher Education through INSINAS Riset Pratama (No. 47/INS-1/PPK/E4/2018 and No. 35/INS-1/PPK/E4/2019) funding scheme.

Institutional Review Board Statement: Not applicable.

Informed Consent Statement: Not applicable.

Data Availability Statement: Data is contained within the article or supplementary materials.

Conflicts of Interest: The authors declare no conflict of interest.

References

1. Diguna, L.J.; Tjahjana, L.; Darma, Y.; Zeng, S.; Wang, H.; Birowosuto, M.D. Light-Matter Interaction of Single Quantum Emitters with Dielectric Nanostructures. *Photonics* **2018**, *5*, 14. [\[CrossRef\]](#)
2. Diguna, L.J.; Darma, Y.; Birowosuto, M.D. The coupling of single-photon exciton-biexciton quantum dot and cavity. *J. Nonlinear Opt. Phys. Mater.* **2017**, *26*, 1750029. [\[CrossRef\]](#)
3. Diguna, L.J.; Hardhienata, H.; Arramel; Birowosuto, M.D. Design of perovskite photonic crystals for emission control. *J. Phys. Conf. Ser.* **2019**, *1170*, 012003. [\[CrossRef\]](#)
4. Diguna, L.J.; Murakami, M.; Sato, A.; Kumagai, Y.; Ishihara, T.; Kobayashi, N.; Shen, Q.; Toyoda, T. Photoacoustic and Photoelectrochemical Characterization of Inverse Opal TiO₂ Sensitized with CdSe Quantum Dots. *Jpn. J. Appl. Phys.* **2006**, *45*, 5563. [\[CrossRef\]](#)
5. Diguna, L.J.; Shen, Q.; Toyoda, T. High efficiency of CdSe quantum-dot-sensitized TiO₂ inverse opal solar cells. *Appl. Phys. Lett.* **2017**, *91*, 023116. [\[CrossRef\]](#)
6. Giménez, S.; Mora-Seró, I.; Macor, L.; Guijarro, N.; Lana-Villarreal, T.; Gómez, R.; Diguna, L.J.; Shen, Q.; Toyoda, T.; Bisquert, J. Improving the performance of colloidal quantum-dot-sensitized solar cells. *Nanotechnology* **2009**, *20*, 295204. [\[CrossRef\]](#)
7. Li, P.; Wei, Z.; Wu, T.; Peng, Q.; Li, Y. Au-ZnO Hybrid Nanopyramids and Their Photocatalytic Properties. *J. Am. Chem. Soc.* **2011**, *133*, 5660–5663. [\[CrossRef\]](#)
8. Justh, N.; Bakos, L.P.; Hernádi, K.; Kiss, G.; Réti, B.; Erdélyi, Z.; Párditka, B.; Szilágyi, I.M. Photocatalytic hollow TiO₂ and ZnO nanospheres prepared by atomic layer deposition. *Sci. Rep.* **2017**, *7*, 4337. [\[CrossRef\]](#)
9. Chen, X.; Li, Y.; Pan, X.; Cortie, D.; Huang, X.; Yi, Z. Photocatalytic oxidation of methane over silver decorated zinc oxide nanocatalysts. *Nat. Commun.* **2019**, *7*, 12273. [\[CrossRef\]](#)
10. Srikant, V.; Clarke, D.R. On the optical band gap of zinc oxide. *J. Appl. Phys.* **1998**, *83*, 5447–5451. [\[CrossRef\]](#)
11. Wojnarowicz, J.; Chudoba, T.; Koltsov, I.; Gierlotka, S.; Dworakowska, S.; Lojkowski, W. Size control mechanism of ZnO nanoparticles obtained in microwave solvothermal synthesis. *Nanotechnology* **2019**, *29*, 06561. [\[CrossRef\]](#) [\[PubMed\]](#)
12. Pimentel, A.; Ferreira, S.H.; Nunes, D.; Calmeiro, T.; Martins, R.; Fortunato, E. Microwave Synthesized ZnO Nanorod Arrays for UV Sensors: A Seed Layer Annealing Temperature Study. *Materials* **2016**, *9*, 299. [\[CrossRef\]](#) [\[PubMed\]](#)
13. Samadipakchin, P.; Mortaheb, H.R.; Zolfaghari, A. ZnO nanotubes: Preparation and photocatalytic performance evaluation. *J. Photochem. Photobiol. A Chem.* **2017**, *337*, 91. [\[CrossRef\]](#)
14. Zhang, Y.; Ram, M.K.; Stefanakos, E.K.; Goswami, Y.D. Synthesis, Characterization, and Applications of ZnO Nanowires. *J. Nanomater.* **2012**, *12*, 624520. [\[CrossRef\]](#)
15. Wang, Y.F.; Shao, Y.C.; Hsieh, S.H.; Chang, Y.K.; Yeh, P.H.; Hsueh, H.C.; Chiou, J.W.; Wang, H.T.; Ray, S.C.; Tsai, H.M.; et al. Origin of magnetic properties in carbon implanted ZnO nanowires. *Sci. Rep.* **2018**, *8*, 7758. [\[CrossRef\]](#) [\[PubMed\]](#)

16. Nurfani, E.; Purbayanto, M.A.K.; Akutsu, R.; Naradipa, M.A.; Diguna, L.J.; Birowosuto, M.D.; Takase, K.; Rusydi, A.; Darma, Y. Tuning the excitonic properties of ZnO:Sn thin films. *Opt. Mater.* **2019**, *88*, 111–116. [[CrossRef](#)]
17. Barakat, M.A. The pyrometallurgical processing of galvanizing zinc ash and flue dust. *J. Miner. Met. Mater. Soc.* **2003**, *55*, 26–29. [[CrossRef](#)]
18. Kusumaningrum, R.; Fitroturokhmah, A.; Sinaga, G.S.T.; Wismogroho, A.S.; Widayatno, W.B.; Diguna, L.J.; Amal, M.I. Study: Leaching of zinc dust from electric arc furnace waste using oxalic acid. *IOP Conf. Ser. Mater. Sci. Eng.* **2019**, *478*, 012015. [[CrossRef](#)]
19. Diguna, L.J.; Shen, Q.; Sato, A.; Katayama, K.; Sawada, T.; Toyoda, T. Optical absorption and ultrafast carrier dynamics characterization of CdSe quantum dots deposited on different morphologies of nanostructured TiO₂ films. *Mater. Sci. Eng. C* **2007**, *27*, 1514–1520. [[CrossRef](#)]
20. Shen, Q.; Kobayashi, J.; Diguna, L.J.; Toyoda, T. Effect of ZnS coating on the photovoltaic properties of CdSe quantum dot-sensitized solar cells. *J. Appl. Phys.* **2008**, *103*, 084304. [[CrossRef](#)]
21. Sahu, D.; Panda, N.R.; Acharya, B.S. Effect of Gd doping on structure and photoluminescence properties of ZnO nanocrystals. *Mater. Res. Express* **2017**, *4*, 114001. [[CrossRef](#)]
22. Aragonès, A.C.; Palacios-Adrós, A.; Caballero-Briones, F.; Sanz, F. Study and improvement of aluminium doped ZnO thin films: Limits and advantages. *Electrochim. Acta* **2013**, *109*, 117–124. [[CrossRef](#)]
23. Ham, H.W.; Kim, Y.S. Theoretical study of indoline dyes for dye-sensitized solar cells. *Thin Solid Film.* **2010**, *518*, 6558–6563. [[CrossRef](#)]
24. Cheng, H.-M.; Hsieh, W.-F. Electron transfer properties of organic dye-sensitized solar cells based on indoline sensitizers with ZnO nanoparticles. *Nanotechnology* **2010**, *21*, 485202. [[CrossRef](#)] [[PubMed](#)]
25. Choi, S.; Phillips, M.R.; Aharonovich, I.; Pornsuwan, S.; Cowie, B.C.C.; That, C.T. Photophysics of point defects in ZnO nanoparticles. *Adv. Opt. Mater.* **2015**, *3*, 821. [[CrossRef](#)]
26. Inamdar, D.Y.; Vaidya, S.R.; Mahamuni, S. On the photoluminescence emission of ZnO nanocrystals. *J. Exp. Nanosci.* **2014**, *9*, 533–540. [[CrossRef](#)]
27. Brillson, L.J.; Lu, Y. ZnO Schottky barriers and Ohmic contacts. *J. Appl. Phys.* **2011**, *109*, 121301. [[CrossRef](#)]
28. Azizah, N.; Muhammadiyah, S.; Purbayanto, M.A.K.; Nurfani, E.; Winata, T.; Sustini, E.; Widita, R.; Darma, Y. Influence of Al doping on the crystal structure, optical properties, and photodetecting performance of ZnO film. *Prog. Nat. Sci.* **2020**, *30*, 28–34. [[CrossRef](#)]